

HEBS and Binary 1-sinc² masks Simulations, HCIT Experiments & Results

May 06, 2005

Table of Contents

I. Introduction

II. Occulting Mask Designs

- II. 1. HEBS Mask Design
- II. 2. Binary Mask Design
- II. 3. Simulations and Expected Results

III. HEBS Mask Fabrication

IV. Measurements on HEBS mask material: Optical constants, OD, Phase

V. Binary mask fabrication

VI. HCIT test set up and details

- VI. 1. HCIT Coronagraph System details
- VI. 2. Experimental Results & Comparison with simulations

VII. Summary

Contributors

**Bala K. Balasubramanian
Dan Hoppe
Dan Wilson
Pierre Echternach
John Trauger
Peter Halverson
Al Niessner
Fang shi
Andrew Lowman**

Jet Propulsion Laboratory

HEBS and Binary 1-sinc² masks

Simulations, HCIT Experiments & Results

May 06, 2005

I. Introduction

Based on preliminary experiments and results with a binary 1-sinc² mask in the HCIT early in August 2004, we planned for a detailed experiment to compare the performance of HEBS and Binary masks under nearly identical conditions in the HCIT. Both types of masks were designed and fabricated and experiments were commenced in December 2004 and continued through January 2005 when very encouraging contrasts with both masks were obtained. This report details the design and fabrication of the masks, simulated predictions, and experimental results.

II. Occulting Mask Designs

Occulting focal plane masks operate in conjunction with a Lyot stop to suppress the starlight in a coronagraphic telescope [Kuchner and Spergel]. In general, these masks are designed and analyzed using Fourier Optics [Goodman]. In the limit of Fourier Optics, these masks can easily be designed to reject the starlight in the regions of interest to below 10^{-10} (-100 dB), the nominal Terrestrial Planet Finder (TPF) requirement [Kuchner, and Traub]. Band-limited binary masks to meet such a requirement, are described in detail by Kuchner. Figure 1 shows a conceptual drawing of a coronagraph with focal plane mask and Lyot stop.

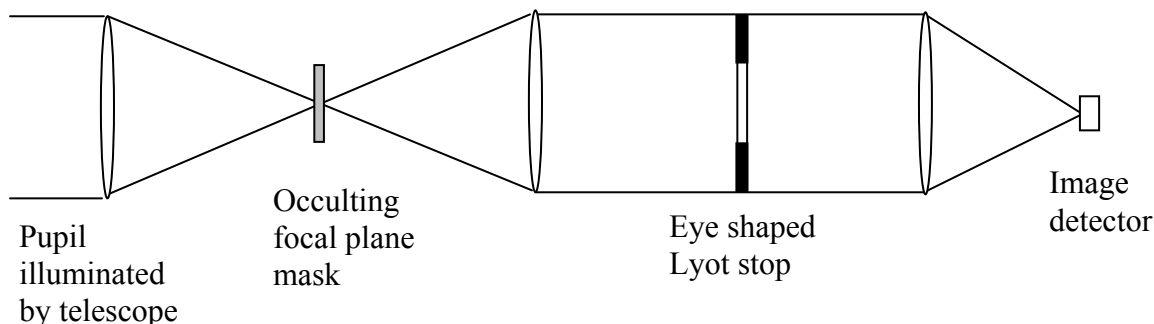


Figure 1. Conceptual drawing of the HCIT coronagraph with occulting focal plane mask

II.1 HEBS Mask Design

Analog gray scale masks based on a special high energy electron beam sensitive (HEBS) glass (Canyon Materials, Inc. San Diego CA, <http://canyonmaterials.com>) can be designed to work as focal plane occulting masks to achieve the required suppression of star light through iterative development of the material, design, and fabrication. For early work on this material, refer to Wilson et al. HEBS material characterization employing spectrophotometry, interferometry and ellipsometry during 2004 can be found in TPF library collection 1864 [Balasubramanian, et al., Jan 2005].

The HEBS mask for the experiment reported here was designed to the following specification by John Trauger (October 25, 2004).

HEBS mask specifications

The spots are positioned on a 17mm x 30mm HEBS glass (nominally 90 mil thick, i.e., 2.28mm) as indicated in figure 2:

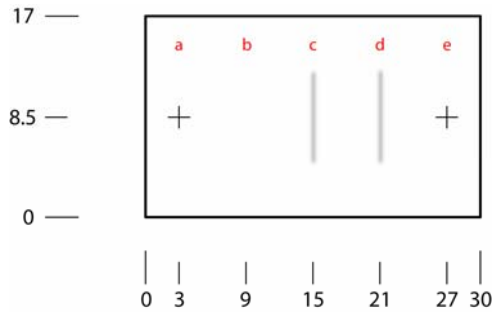


Figure 2. HEBS mask patterns layout on a 17mm x 30mm HEBS glass

The pattern locations are as follows:

- a) Fiducial mark, a pair of 10 μ m-wide lines in the form of a '+'
- b) Blank
- c) Linear sinc² profile (c), with pattern length of 8 mm
- d) Linear sinc² profile (d), with pattern length of 8 mm
- e) Fiducial mark, a pair of 10 μ m-wide lines in the form of a '+'

The specified mathematical profiles are as follows:

$$\text{Profile (c)} \quad T(r) = T_0 \left[1 - \left(\frac{\sin(\pi x/w)}{(\pi x/w)} \right)^2 \right]^2$$

Note: $w = 157.7 \mu\text{m} \Rightarrow T(x) = 0.5 T_0$ at $x = 90.3 \mu\text{m}$
Set $T(x) = 1.0$ for all $|x| > 7 \times 157.7 = 1.104 \text{ mm}$

$$\text{Profile (d)} \quad T(r) = T_0 \left[1 - \left(\frac{\sin(\pi x/w)}{(\pi x/w)} \right)^2 \right]^2$$

Note: $w = 118.2 \mu\text{m} \Rightarrow T(x) = 0.5 T_0$ at $x = 67.7 \mu\text{m}$
Set $T(x) = 1.0$ for all $|x| > 8 \times 118.2 = 945.9 \mu\text{m}$

For reference: The sinc² profile $[1 - (\sin(\pi z)/(\pi z))^2]^2 = 0.5$ at $z = 0.57283$

These profiles were designed for F# 28.55 and wavelength 785nm

References:

- Kuchner and Traub, A coronagraph with a band-limited mask for finding terrestrial planets, ApJ 570, (2002) pp. 900-908
- Trauger et al., Coronagraph contrast demonstrations with the High Contrast Imaging Testbed, SPIE 5487, (2004), pp. 1330-1336
- Wilson et al., Eclipse apodization: realization of occulting spots and Lyot masks, SPIE 4860, (2003), pp. 361-370

II. 2. Binary Mask Design

In the case of binary masks, an analog band-limited function such as Sin^2 or $1-\text{Sinc}^2$ is sampled and a series of apertures is created that mimics the throughput of the analog mask. The mask is referred to as binary since it consists only of perfectly blocking metal and totally transmitting empty apertures (0/1). If the parent function is periodic then the resulting binary mask will also be periodic in the search direction (x). If the parent function is non-periodic, such as $1-\text{Sinc}^2$, then the binary mask is non-periodic in the search direction. Both types of binary mask are chosen to be periodic in the non-search direction (y), with a period of $F\#\lambda$, where $F\#$ is the focal length/diameter ratio of the telescope and λ is the operating wavelength. Typical inner working angles (IWA) values are in the range of 3-5 (λ/D) for the TPF mission. In addition to the two-dimensional aperture distribution of the mask the metal layer will have some finite, and non-negligible thickness, for a practical mask. Since these masks are placed in the image plane they will be illuminated by an Airy disk in the spatial domain, or equivalently a cone of rays in the spectral domain. Figures 3 and 4 depict a typical $1-\text{Sinc}^2$ binary mask.

A detailed discussion on the binary mask design concept and the effects of metal thickness, wavelength, polarization etc are presented in the attached document (Dan Hoppe, May 2005, 2005; see TPF library collection # 1864).

To match the performance of the above HEBS mask designs, binary masks were designed for the same $F\#$ and wavelength as per the following specifications. The layout of the patterns as fabricated on a 90 mil thick fused silica glass are shown in Figure 19 in the section on fabrication.

The binary mask profiles are as follows:

$$h(x) = P_y \left[1 - \sqrt{T_0} \left(1 - \frac{\left(\sin\left(\frac{\pi x}{w}\right) \right)^2}{\left(\frac{\pi x}{w}\right)} \right) \right]$$

$$T_0 = \sqrt{0.9}$$

$$-4.0\text{mm} < y < 4.0\text{mm}$$

$$P_y = F * \lambda = 22.41\mu\text{m}$$

$$h_{\min} = P_y \left[1 - \sqrt{T_0} \right] = 1.15\mu\text{m}$$

Mask #1
(pattern 3
in layout): $w = 157.7\mu\text{m}$
 $-7 * w < x < 7 * w$

Mask #2
(pattern 6 in
layout): $w = 118.2\mu\text{m}$
 $-8 * w < x < 8 * w$

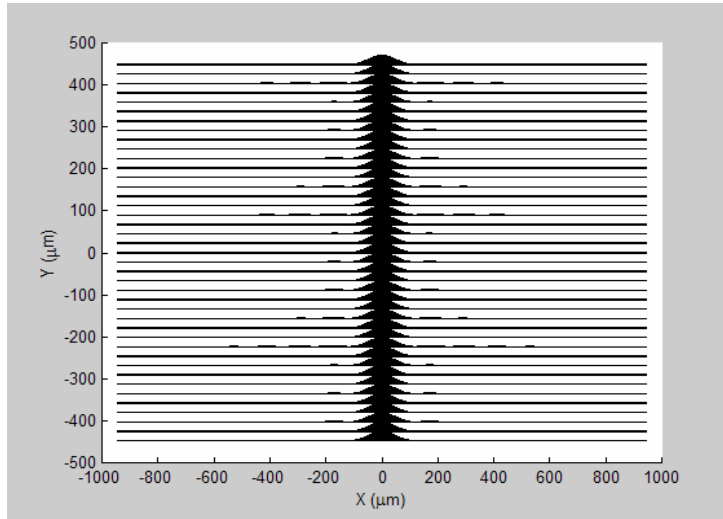


Figure 3: Binary 1-sinc² mask pattern

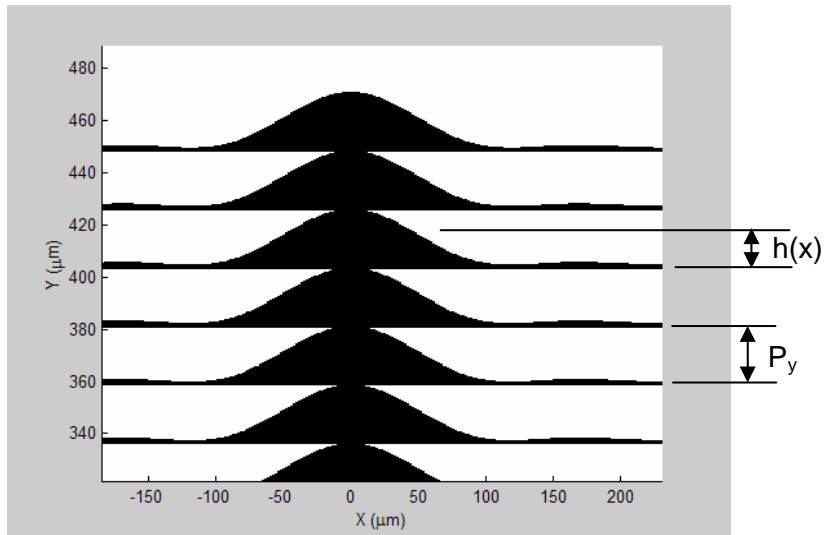


Figure 4: Detailed view of Binary 1-sinc² mask pattern

II.3. Simulations and expected results

Refer to Dan Hoppe's detailed reports on mask designs and contrast simulation included in the TPF library collection 1864 [Hoppe, (1) Performance predictions of binary masks to be tested in HCIT, July 2004, (2) Full wave analysis of binary masks, July 2004, (3) Binary_Sinc2_Masks_DJH, May 2005]. Some salient predictions in comparison with experimental results are presented in section VI.2 below.

III. HEBS Mask Fabrication

The HEBS glass as produced by Canyon Materials Inc., consists of a 10 micron thick high energy electron beam sensitive layer on both sides of a 90 mil thick glass plate which is nominally similar to BK7 in optical characteristics (see differences in figure 12). The sensitive layer gets darkened to various levels of optical density when exposed to electron beam irradiation at chosen doses. Specific transmission profiles can be obtained on such a glass when the electron beam energy is preprogrammed to match a required pattern. The patterns are written with a high precision electron beam lithography system (JEOL 9300FSZ Electron Beam Lithography at Micro Devices Lab; figure 5). Calibration runs guide the correct choice of e-beam exposure parameters such as current, exposure time etc to achieve a desired optical density at a specific location on a mask.

Pattern preparation process for all profiles described here:

1. Pixelize the transmittance (T) or optical density (OD) function profile (typically 1 μm square pixels)
2. Convert pixel ODs into E-beam doses using the measured OD vs. dose calibration curve for the particular glass being used. Because the calibration curve was measured using broad area exposures, it is understood that the measured calibration regions include the proximity (scattered electron) dose. The proximity dose is approximated by a Gaussian function, and hence the point spread function of the total E-beam exposure is $PSF(\mathbf{r}) = \delta(\mathbf{r}) + \eta / (\pi\alpha^2) \exp(-r^2 / \alpha^2)$, where \mathbf{r} is position, and η and α are the proximity effect strength and range, respectively. When we use the dose calibration curve to determine the pixel doses, we are actually finding the desired *total* dose which is the incident dose times $1 + \eta$. A separate set of experiments was performed to infer the approximate range and strength of the proximity effect for this HEBS glass, with the results being $\eta \approx 1$ and $\alpha \approx \mu\text{m}$. This means that the proximity effect contributes approximately the same dose as the incident beam and requires careful compensation to realize accurate transmittance profiles.
3. To determine the incident dose pattern to expose, we use the fact that the total dose is



Minimum beam dia: 4nm at 100kV

Electron beam vector scanning with scan increments down to 1nm

Laser interferometer positioning system with a resolution of 0.62nm

Stitching accuracy between fields better than 20nm.

The acceleration voltage switchable between 50kV and 100kV

Figure 5. E-beam Lithography system employed to fabricate masks at MDL

the convolution of the incident dose with the point-spread function. We can therefore use Fourier transform techniques to deconvolve the proximity effect out of total dose pattern determined in step 2. During deconvolution, it is necessary to add a small background dose to the function to avoid doses smaller than the E-beam tool can deliver at the given current. This is accomplished by setting T_0 to a value less than unity in the function specifications below.

It should be noted that the two-dimensional *PSF* and convolution are simple approximations to a three-dimensional process of electron scattering inside the HEBS glass. We have found that the approximation works very well for analog-relief resist processing, and it appears to be valid for this application as well. As will be seen later, adjustments need to be made to the range and strength parameter values. If this is not accurate enough, a two-component Gaussian function could be tried.

Fabrication Process for all HEBS glass occulting spots described here

1. Thermally evaporate 200Å chrome to serve as an E-beam discharge layer
2. E-beam expose pattern with the following parameters:
Acceleration voltage = 100kV
Current = 1 nA
Spot-to-spot step size = 50 nm
Spot size \approx 150 nm (slight defocus)
Expose all patterns in 5 passes at 1/5 dose to achieve good uniformity (bulk charging/heating was shown to be a problem). All patterns in the job are written before returning to write the next pass.
3. Remove chrome in Cyantek CR-7S Chromium Etchant
4. Clean plate in Alconox detergent and rinse with deionized water.

Transmission Images of Fabricated Spots

Imaging system setup:

- Oriel monochromator set to output 785 nm light (slits quite wide, so probably at least 5 nm bandwidth)
- Collimating/focusing lens
- HEBSPT10 occulting mask
- 20x microscope objective with C-mount adapter

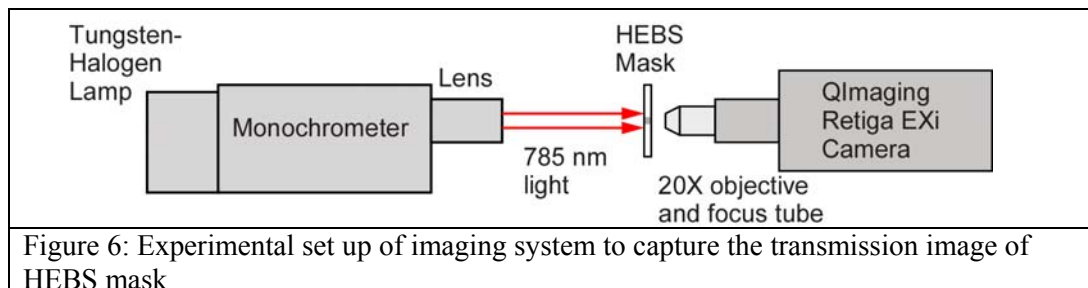


Figure 6: Experimental set up of imaging system to capture the transmission image of HEBS mask

- C-mount focusing tube (Edmund Optics, ~2" long)
- QImaging Retiga EXi CCD camera (1392x1040, 6.45 μm x 6.45 μm pixels, 12 bit, TE cooled 25°C below ambient)
- Setup is non-optimal in that the illumination should be focused to match the imaging objective to minimize scattering and improve resolution.
- Improved images can be obtained by aperturing the HEBS mask so that only the occulting spot is transmitting.

Image capture and processing:

1. Capture and average 4 images of the following: a) the occulting spot, b) an unexposed region of glass (to correct for illumination non-uniformity), and c) dark images
2. Calculate transmission images using the following formula

$$T = \frac{I_{spot} - I_{dark}}{I_{nospot} - I_{dark}}$$

3. Average 50 rows of the transmission image and compare to the specified functional forms. The magnification of the microscope system was estimated using test exposures of known size on the same piece of glass. When comparing the functions to the measured data, scaling of the analytical function T_0 was allowed to obtain the best fit.

Transmission image of typical profile (not the exact sample fabricated on October 27th and tested in HCIT):

sinc^2 mask with $w = 141.9 \mu\text{m}$

Fabrication: $T_0 = 0.90$, Pixel size = 1.25 μm , Proximity effect strength, $\eta = 1.6$

Profile (b) shown in figure $T(x) = T_0 \left[1 - \left(\frac{\sin(\pi x/w)}{(\pi x/w)} \right)^2 \right]^2$

With: $w = 141.9 \mu\text{m}$

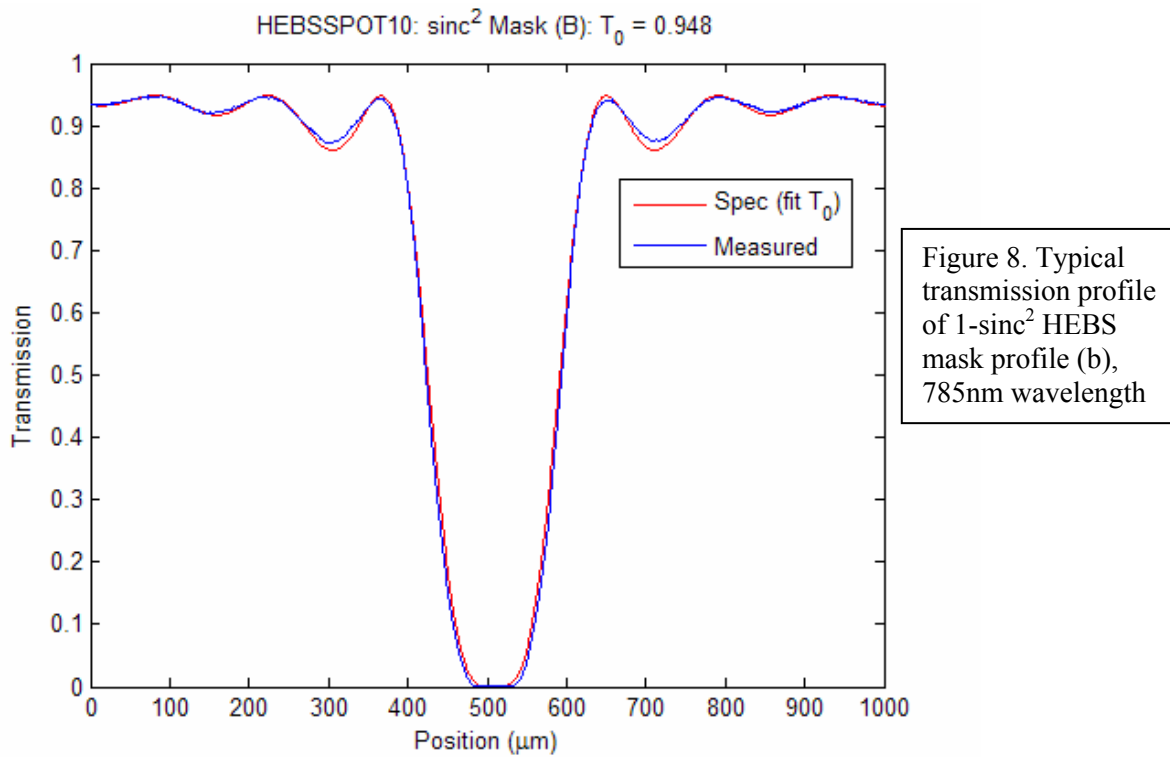
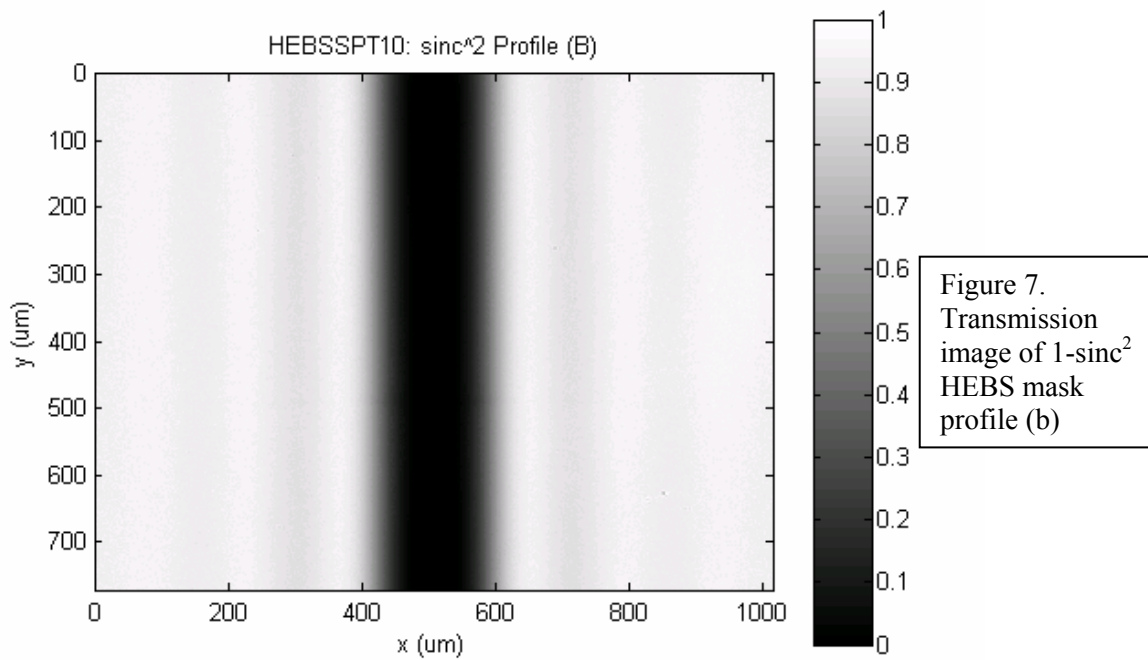
$\Rightarrow T(x) = 0.5 T_0$ at $x = 81.3 \mu\text{m}$

Set $T(x) = 1.0$ for all $|x| > 1.20 \text{ mm}$

$T_0 = 0.90$, Pixel size = 1.25 μm , Proximity effect strength, $\eta = 1.6$

Comments:

- a. The amplitude of the oscillations needs to be improved. We tried increasing the proximity effect strength from 1 to 1.6, but the profile did not improve significantly, so perhaps the proximity range (currently 20 μm) is being underestimated.
- b. The fit value of T_0 does not match that used in the fabrication specification (fit value is higher), so the glass calibration may be off. Perhaps we need to recalibrate using the same current/exposure scheme as when the spots are written.



IV. Measurements on HEBS mask material: Optical constants, OD, Phase

The optical density and transmitted light phase retardation were measured with an interferometer specially designed and setup for the purpose at JPL. Special samples were fabricated with chosen series of OD regions to help make these measurements. Two such samples are shown in figures 9, and 10 on which the optical densities and phase advances have been measured.

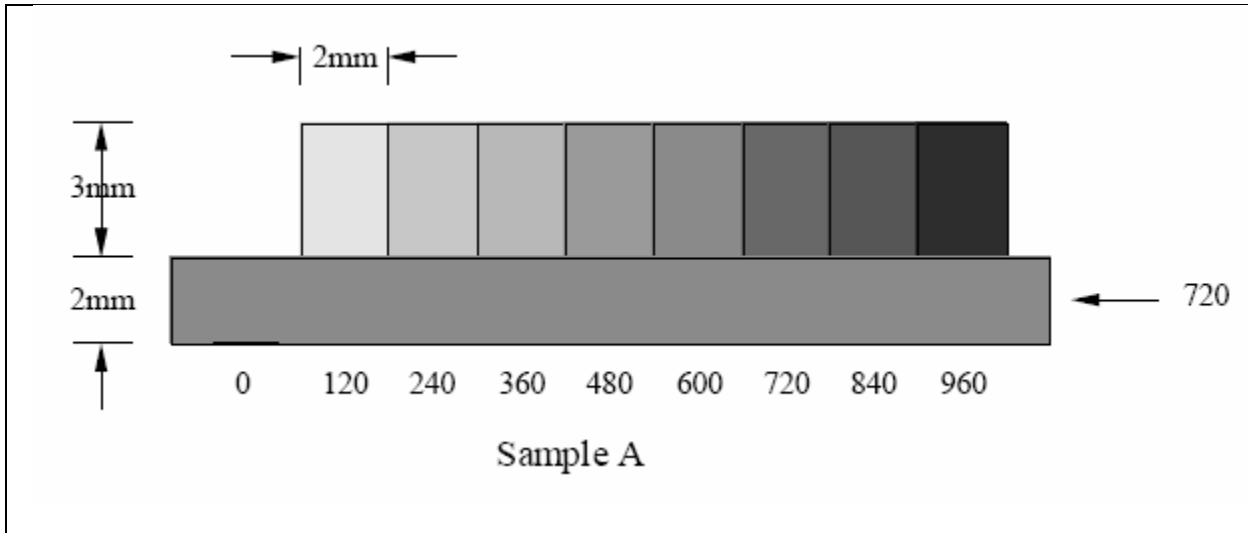


Figure 9. HEBS Sample A for measuring OD and phase retardation. Exposure levels are shown against the rectangular regions in microcoulombs/cm²

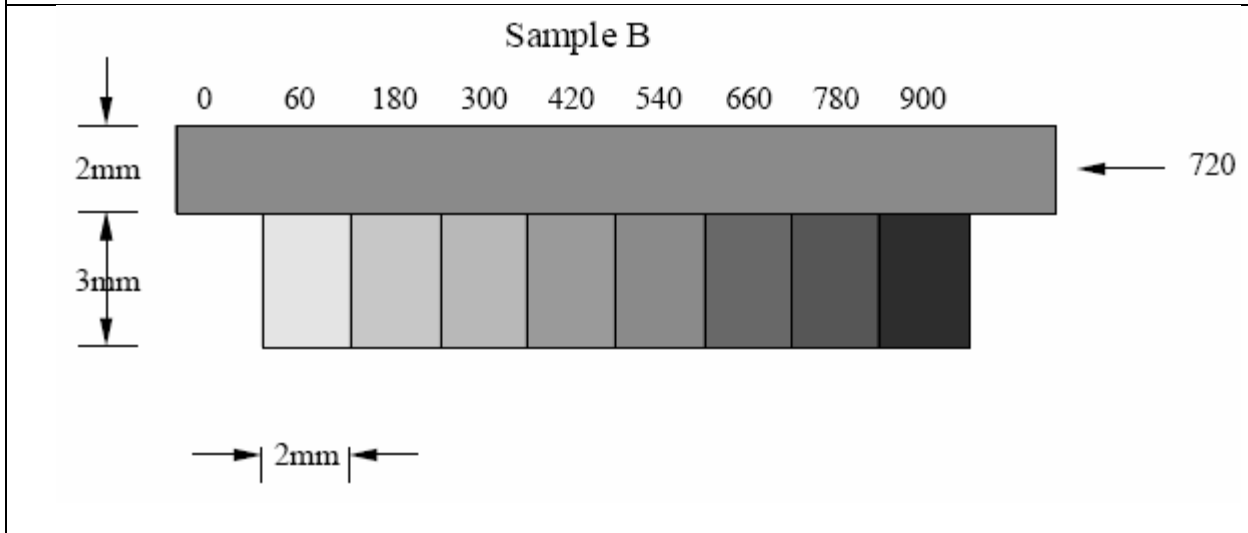


Figure 10. HEBS Sample B for measuring OD and phase retardation. Exposure levels are shown against the rectangular regions in microcoulombs/cm²

Figure 11 shows the interferometer system used to make the phase and OD measurements. Measured optical density vs. dose and phase advance or retardation vs. optical density at 532nm, 635nm, 785nm and 830nm wavelengths are shown in figures 16 and 17. Reliable measurement of OD and phase retardation for OD >4 is a subject of on-going research because of the noisy nature of these measurements at low light levels.

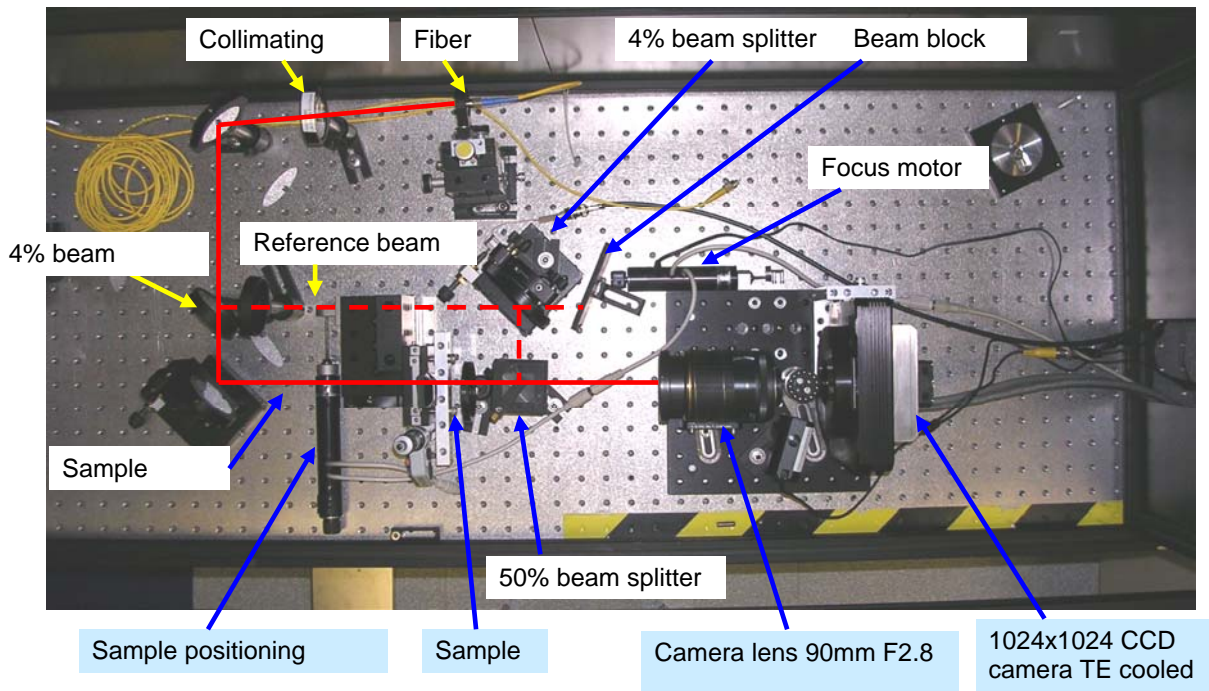


Figure 11. Interferometer system to measure optical phase advance due to HEBS mask

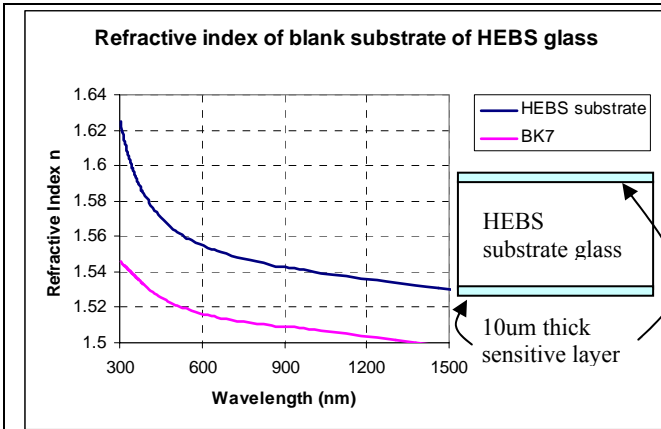


Figure 12. Refractive index of the HEBS substrate as a function of wavelength in comparison with BK7

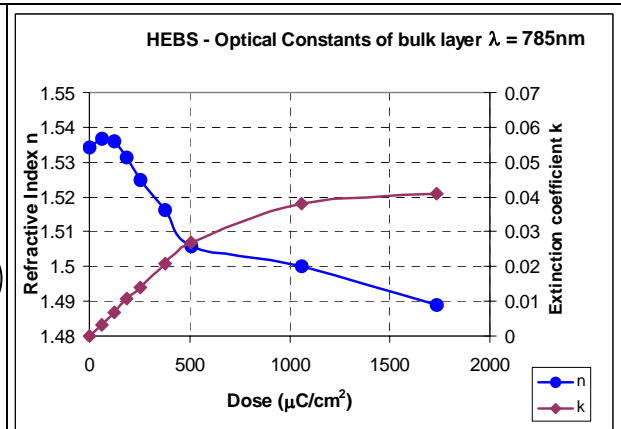


Figure 13. Refractive index and extinction coefficient of HEBS sensitive layer

Refractive index vs. wavelength of the HEBS substrate measured by ellipsometry is shown in figure 12 to compare with that of BK7. Models suggest that a top surface layer of about 150nm thickness with a graded index profile through thickness exists on the 10.5 micron thick HEBS layer and it varies with the exposure; figure 13 shows the refractive index and extinction coefficient at 785nm wavelength for the rest of the bulk layer. Note that the refractive index increases initially and then drops with exposure. Only one side layer is sensitized by e-beam to create the mask profile. The other side remains transparent. Due to the finite thickness of the sensitive layer, a weak interference oscillation with wavelength is seen in transmission and reflection; polishing and AR coating the unsensitized side will reduce this effect.

Figures 14 and 15 show the dispersion characteristics of the sensitive layer of HEBS material for various levels of electron beam exposures that produce absorption to various optical densities as shown in figure 16. The optical constants were derived from ellipsometric measurements at J.A. Woollam Co Inc. with a variable angle spectroscopic ellipsometer (VASE). Further details of these measurements can be found in the document “HEBS Mask Material Characterization Dec 18, 2004 v2.pdf” in TPF library collection #1864.

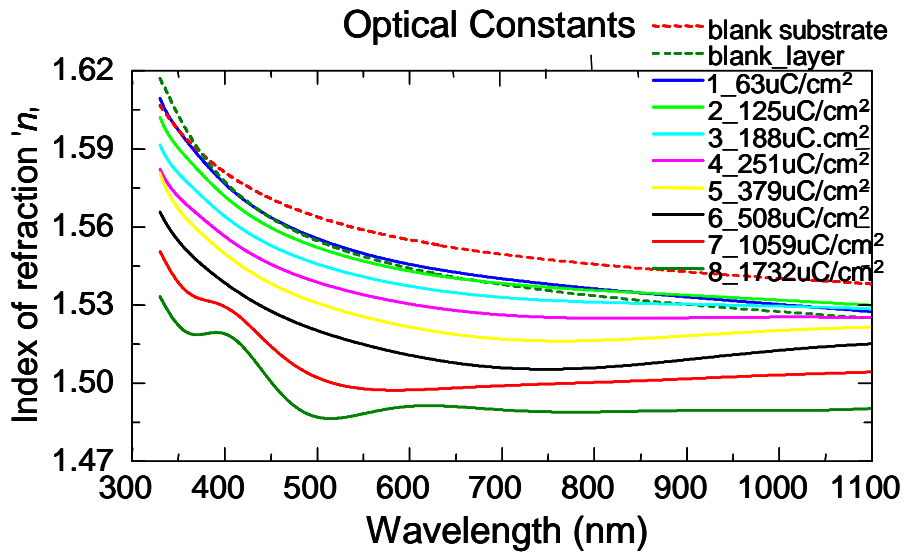


Figure 14. Refractive index of the sensitive HEBS layer as a function of wavelength for various of electron beam exposure levels

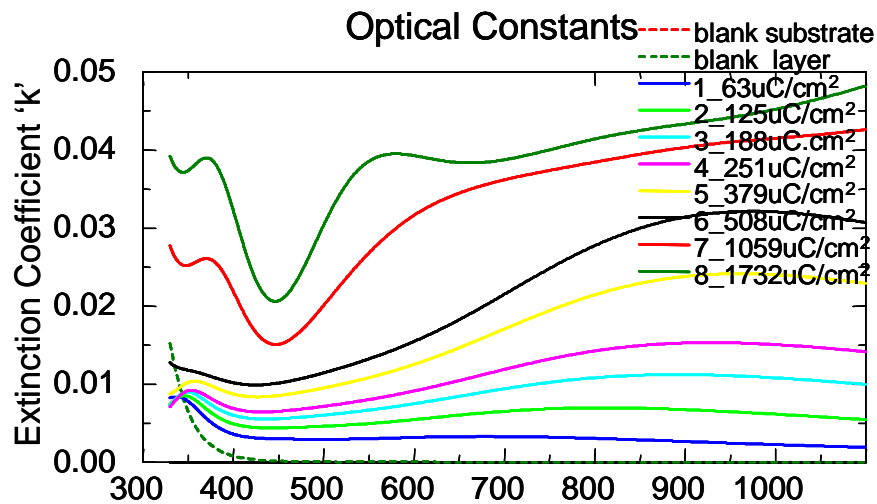


Figure 15. Extinction coefficient of the sensitive HEBS layer as a function of wavelength for various electron beam exposure levels

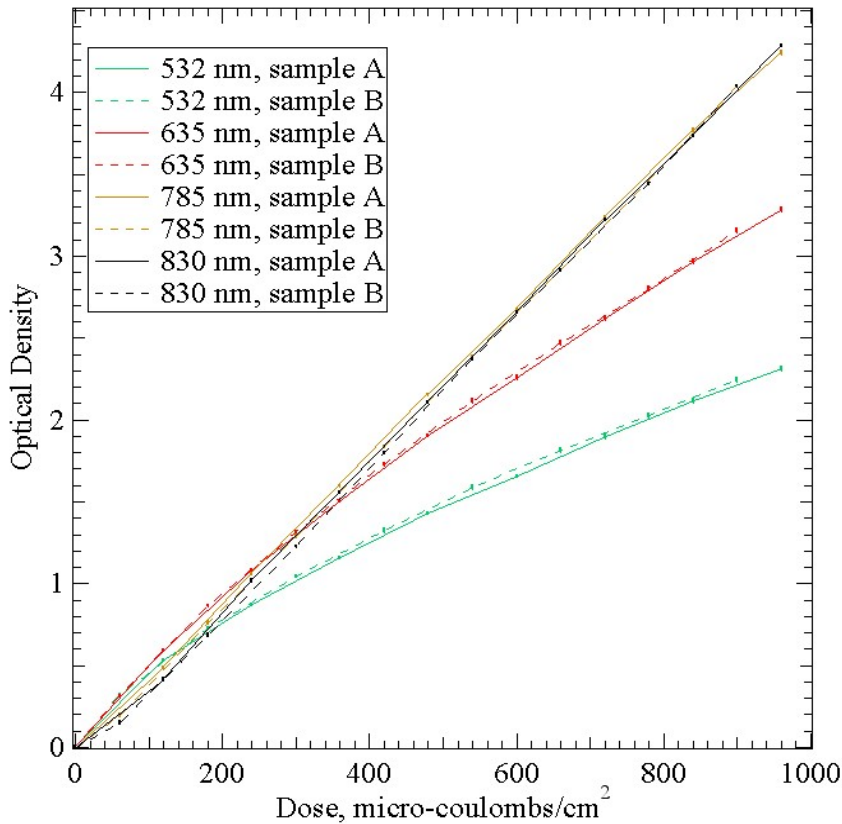


Figure 16.
Optical density
vs. electron
beam exposure.

For OD, the error bars (not easily seen in these plots) represent the one sigma scatter in average brightness of pixel columns, after correcting for non-uniform illumination of the samples, non-uniform imaging lens throughput and camera sensitivities.

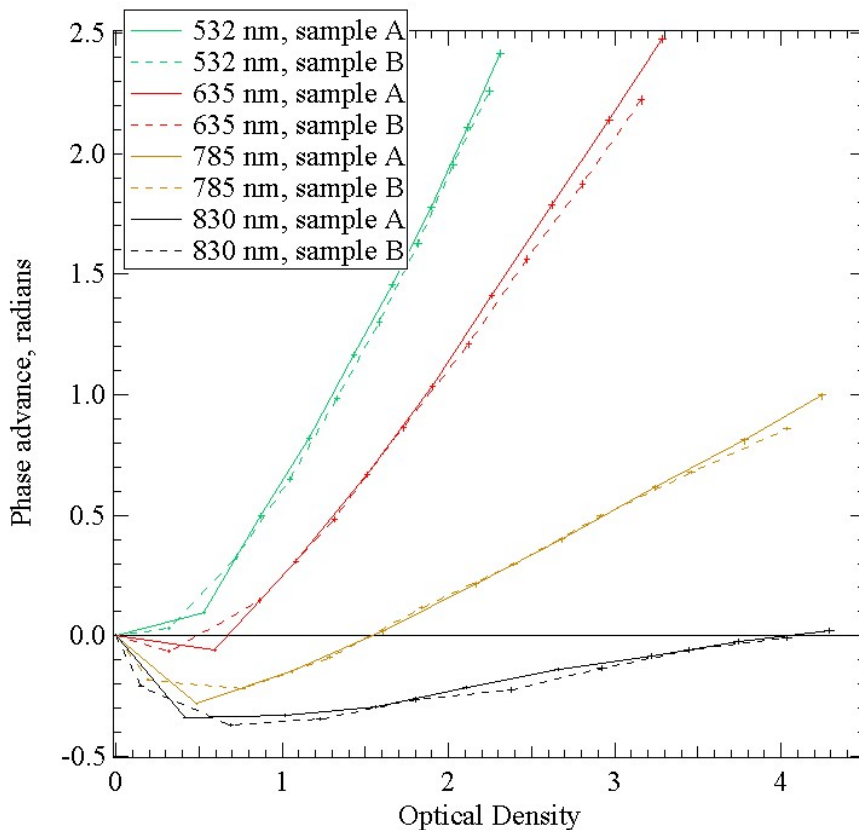


Figure 17.
Phase advance
vs. Optical
Density

For phase, the error bars (not easily seen in these plots) are based on chi-squared likelihood estimates from the polynomial-with-step fit to the phase. The error bars represent the size needed to achieve a 68% probability that the “true” phase step is within the bar’s range.

V. Binary Mask Fabrication

Binary mask patterns are generated by e-beam lithography and lift off process as described below to produce binary mask pattern with nominally 150nm thick aluminum film coated by evaporation on fused silica glass.

Pattern generation

The binary mask patterns are created using the equations provided by programming a script file that is interpreted by the layout programming (L-Edit). A unit cell of the pattern is composed of 10000 trapezoids with width and height dictated by the equations. A cell consisting of three unit cells stacked in the “y” direction is imported into a conversion software that performs proximity correction to correct the e-beam dose at each point of the pattern. Narrow regions of the pattern are assigned lower doses than the wide portions. The center cell of this corrected pattern is then arrayed to compose the total pattern. The conversion software generates a dose table to be used at expose time.

E-beam patterning

The fused silica wafer is coated with two coats of PMMA 950K, 2% in Chlorobenzene, spun at 4000 rpm for 40s and baked at 170C for 10 min. This yields a film thickness of 220 nm. A top layer of resist, 100 nm of ZEP 520 (1:2) in Chlorobenzene is spun at 4000 rpm for 40 seconds and baked at 170C for 10 min on a hot plate. Finally, a 20 nm thick Al discharge layer is evaporated on top of the resist structure using a thermal evaporator. The sample is exposed in the JEOL 9300 electron beam lithography system. The base dose is $170\mu\text{m}^2/\text{cm}^2$. After exposure, the Al discharge layer is removed in AZ400K resist developer. The pattern is developed with p-Xylenes for 60s followed by MIBK:IPA 3:1 for 2 min to develop the PMMA underlayer. The resist bilayer creates an undercut profile to facilitate lift off. The substrate is then placed in the thermal evaporator and 150 nm aluminum is deposited. The last step is the lift-off in acetone. Harsh ultrasonic agitation is not used because of the delicate aluminum structures. Instead, the sample is soaked for at least 24 hours, and the excess aluminum is removed using a gentle acetone spray. The process steps are shown in figure 18.

Samples

Figures 19 and 20 show the binary mask fabricated in Oct. 2004 at the Micro Devices Lab (MDL) in JPL. Similar 8th order masks have been fabricated subsequently in Feb 2005 and are being tested now. Characterization of these binary masks and patterns for phase and amplitude of the zeroth order transmitted beam is being done now; this turns out to be more challenging than anticipated.

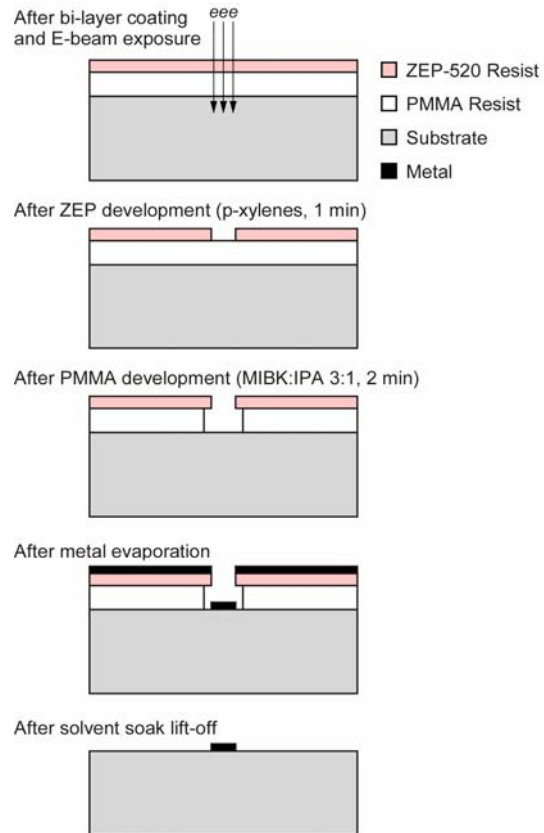


Figure 18. Binary mask fabrication process with e-beam patterning and lift off

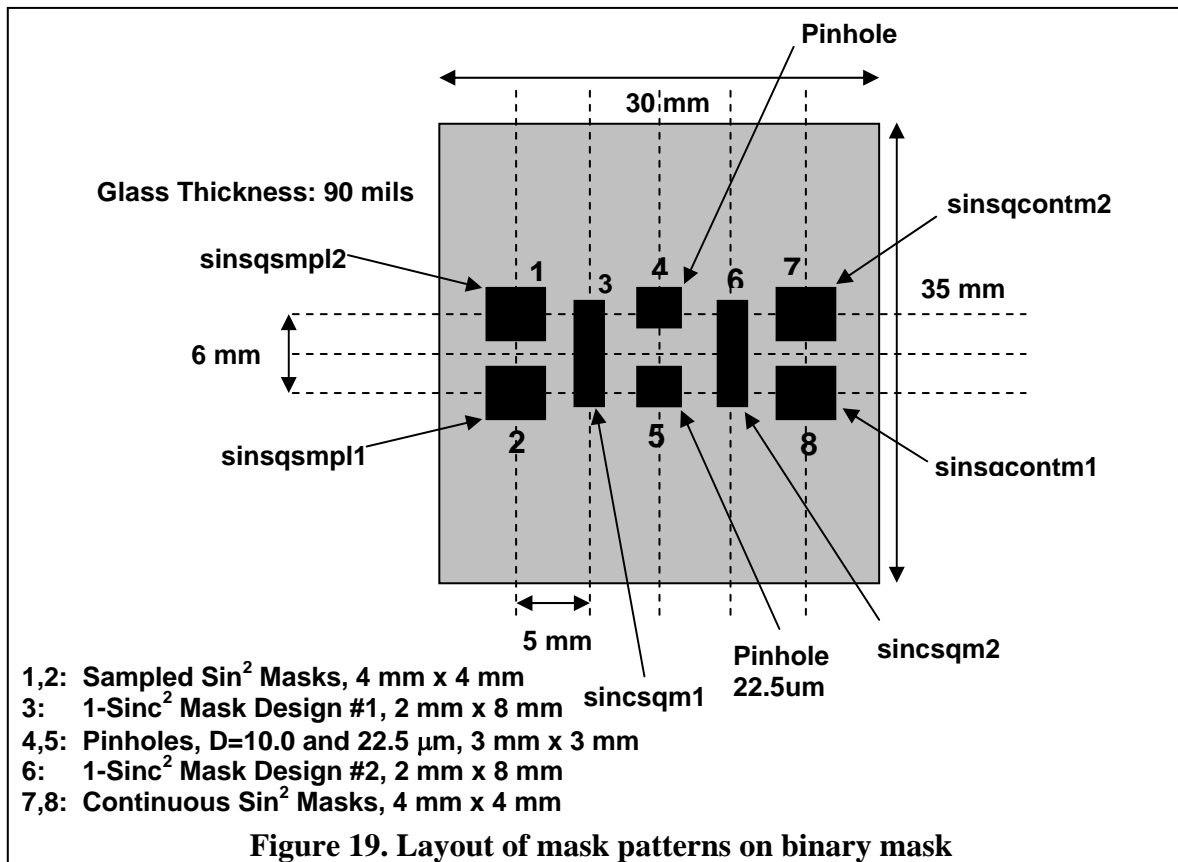


Figure 19. Layout of mask patterns on binary mask

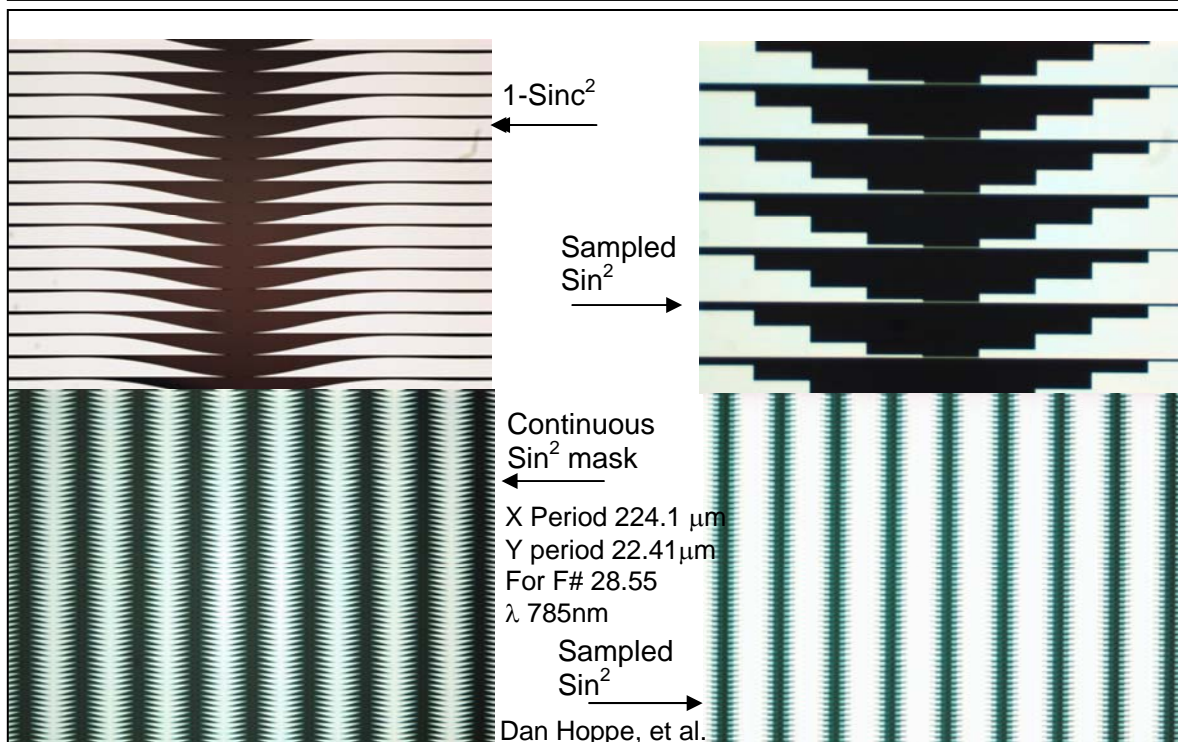


Figure 20. Micro Images of Binary Mask patterns

VI. High Contrast Imaging Testbed (HCIT)

The opto mechanical layout of the HCIT is shown in figure 21. For a detailed account of the test bed set up, refer to John Trauger et al., Proc SPIE 5487, 2004 (included in the TPF library collection 1864). Not shown in the figure is the addition of a calcite polarizer before the final image detector. This polarizer separates the two orthogonally polarized images in slightly offset locations at the image plane. The DM can be optimized to minimize the speckles in either polarization independently, thus estimating the best contrast achievable in one polarization while allowing the other to float. The binary mask is inherently sensitive to polarization and hence this device is helpful in estimating performance in the two polarizations. Other modifications/enhancements to the test bed planned for the future include a front end polarizer, a wide band super continuum source, spectral filters to select various bands, actuators to precisely move Lyot stop in x and y for accurate and optimum positioning, and a fiber scanning system to accurately characterize the field amplitude in Lyot plane.

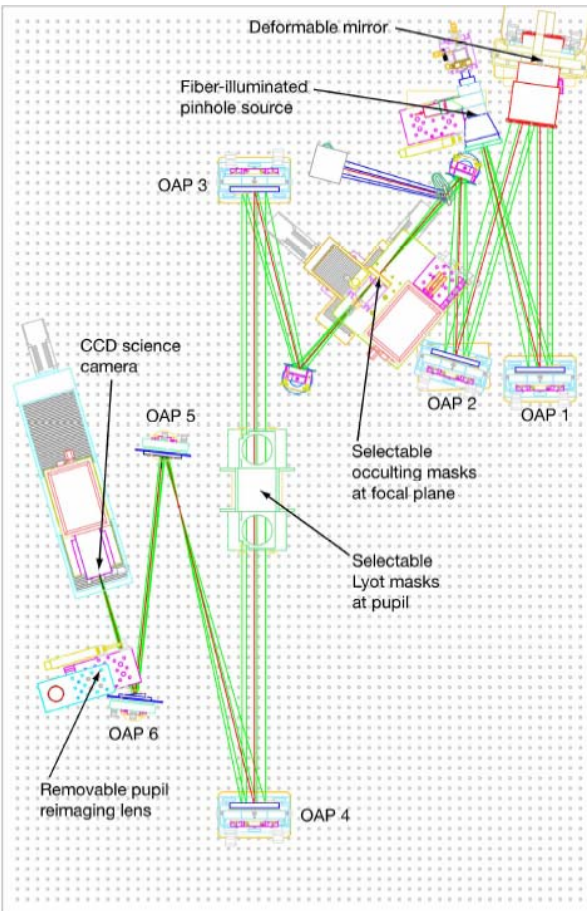


Figure 21. Opto mechanical layout of the High Contrast Imaging Testbed at JPL

VI. 1. HCIT Coronagraph System Details

Optics: Gold coated OAPs and flats
 System F #: 28.55 at the focal plane occulter
 F# at the final image when no stop is employed: 86.55
 Wavelength: 785nm laser light

Additional broadband source (xenon arc) filtered by an optical filter from Barr Associates with +/-40nm bandwidth centered at 800nm with stop band attenuation to OD 6 and peak transmission ~ 90%. This was installed in Dec 2004 replacing an earlier CVI filter which was less efficient in pass band and with larger leakage in the red end of stop band.

Changes in electronics were also implemented in Dec to reduce high frequency noise mainly from computers. Gold coated Xinetics DM 32x32 #5 with PMN actuators were installed on Jan 6, 2005 and used for these experiments reported here. 16 bit multiplexer with 1.5mV/bit give a resolution of 3.5nm/volt with a full range of 100V on the mux but operated to a neighboring actuator safety limit of about 15V around a nominal flatness setting around 20V. The maximum physical displacement between neighboring actuators is thus about 50nm. A thermal shell was installed on Jan 6, 2005 to achieve a thermal stability of about 20-30mK nominally around 23C.

Focus optimization methodologies including speckle nulling at each focus position were implemented and focus sweep experiments were performed to find optimum focus on the mask. The mask mounted on actuators can be moved in 0.5 μm steps in the x axis and 1μm steps in y axis. Currently the mask is mounted at 5 deg tip and has no tip and tilt adjustment. Both HEBS and Binary masks were mounted side by side on one mount to be able to move between the two masks by external control without breaking vacuum and ensuring nearly identical conditions for the two masks during the tests.

Lyot stop: The beam diameter at the pupil and Lyot plane in the HCIT is 27mm. The Lyot stop in the HCIT consists of two circular apertures made in black anodized aluminum disks. The apertures are mounted with their centers displaced in x thus forming an “eye” shaped stop as shown in figure 22 to block the diffracted light through the occulting mask. The chosen circular apertures for the contrast results shown in figures 23 to 29 were of 27mm diameter (D) with 12.15mm center to center separation (L) so that the eye width w = 14.85mm.

$$\text{Area of the eye} = 2(D/2)^2 \cos^{-1}(L/D) - (1/2)L \cdot \sqrt{(D^2 - L^2)}$$

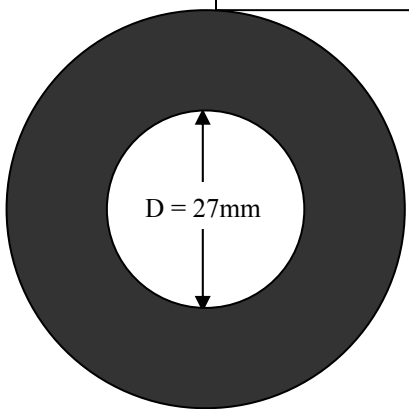
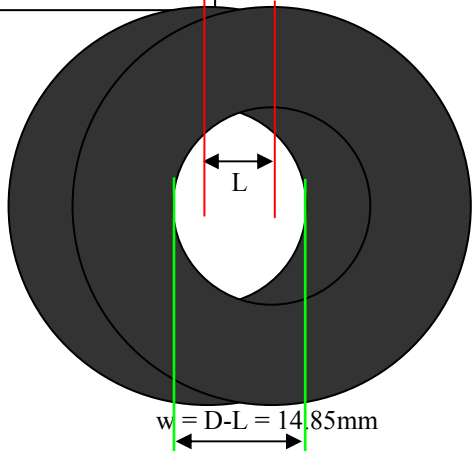


Figure 22. Lyot Stop employed in the HCIT for these experiments. For 27mm dia of open circles and 12.15mm center to center separation, the area of the eye = 255.9sq.mm. Area of 27mm circle = 572.6 sq.mm. Ratio = 45%



VI.2. Experimental Results & Comparison with simulations

HEBS and Binary 1-sinc² masks were fabricated as detailed in previous sections. These masks were placed side by side on one mount in the HCIT and tested. Calibration images without the mask and nulled images with each mask were taken and contrast was calculated as a function of position in the target image being nulled. Results are presented here.

Contrast Calculations:

$$C(x, y) = \frac{I(x, y)_{\text{final image of star with mask and Lyot}}}{M(x, y) \bullet I(0, 0)_{\text{final image of star without mask but with LyotStop}}}$$

where $I(x, y)_{\text{final image of star with mask and Lyot}}$ is the intensity of the final image at a given point (x,y)

$M(x, y)$ is the mask transmission at (x,y)

$I(0, 0)_{\text{final image of star without mask but with Lyot}}$ is the Image intensity at (0,0) of the star with no mask but with Lyot stop

Ideally one should calculate contrast as,

$$C(x, y) = \left(\frac{I(x, y)_{\text{final image of planet}}}{I(x, y)_{\text{final image of star}}} \right)$$

with Mask and Lyot Stop

This will become feasible when a star/planet simulator is built and installed in the HCIT.

HEBS Mask

Figure 23 shows the contrast plot and contrast image obtained with a HEBS 1-sinc² linear occulting mask (figure 2, profile c) with 785nm laser source in the HCIT. An average contrast of 9×10^{-10} has been achieved with a stability of about 5×10^{-11} per hour. Reference: Trauger et al. presentation, TPF/STDT meeting on Feb 24, 2005, JPL – TPF library collection 2911. Similar experiment with the same mask with filtered white light source with 10% band pass centered at 800nm achieved average contrast of 3×10^{-9} in the target box. Figure 24 shows the contrast image and plot for this result. Reference: Trauger et al. presentation, TPF/STDT meeting on Feb 24, 2005, JPL – TPF library collection 2911.

HEBS material exhibits phase retardance or advance for transmitted light with darkening of the glass. Phase vs OD (figure 17) has been measured at JPL with an interferometer as discussed earlier. While this work and detailed studies are in progress, preliminary simulations indicate degradation of contrast due to such unintended phase retardation effects in the mask. However, it is encouraging to note that these effects seem to be within the capability of the DM to correct the field and obtain the level of contrast achieved in the HCIT experiments. Also the HEBS glass exhibits wavelength dependence of basic characteristics of OD and phase. Further development in the mask material together with measurements and simulations is expected to yield insights to improve the performance and broaden the bandwidth. Detailed simulations of the HEBS mask are a subject of on-going investigations.

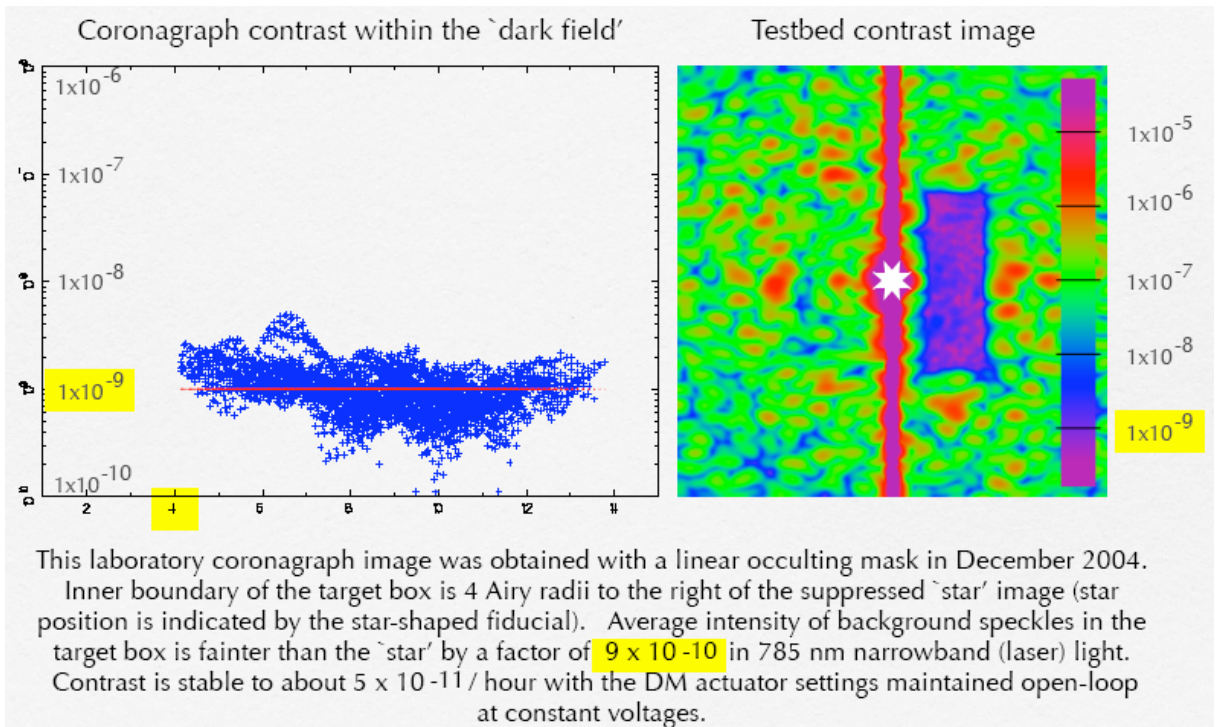


Figure 23. HCIT Contrast vs Airy radius in the target box of 4 to $10\lambda/D$ in x and - 10 to $+10\lambda/D$ in y

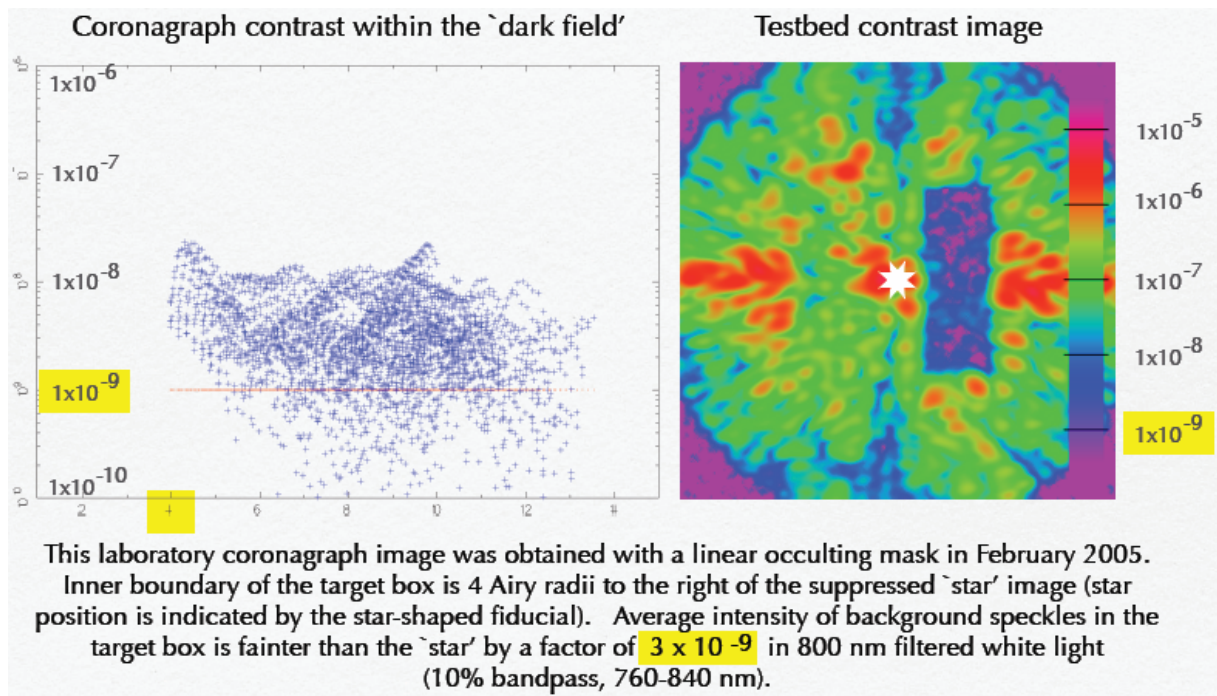


Figure 24. HCIT Contrast vs Airy radius in the target box of 4 to $10\lambda/D$ in x and - 10 to $+10\lambda/D$ in y

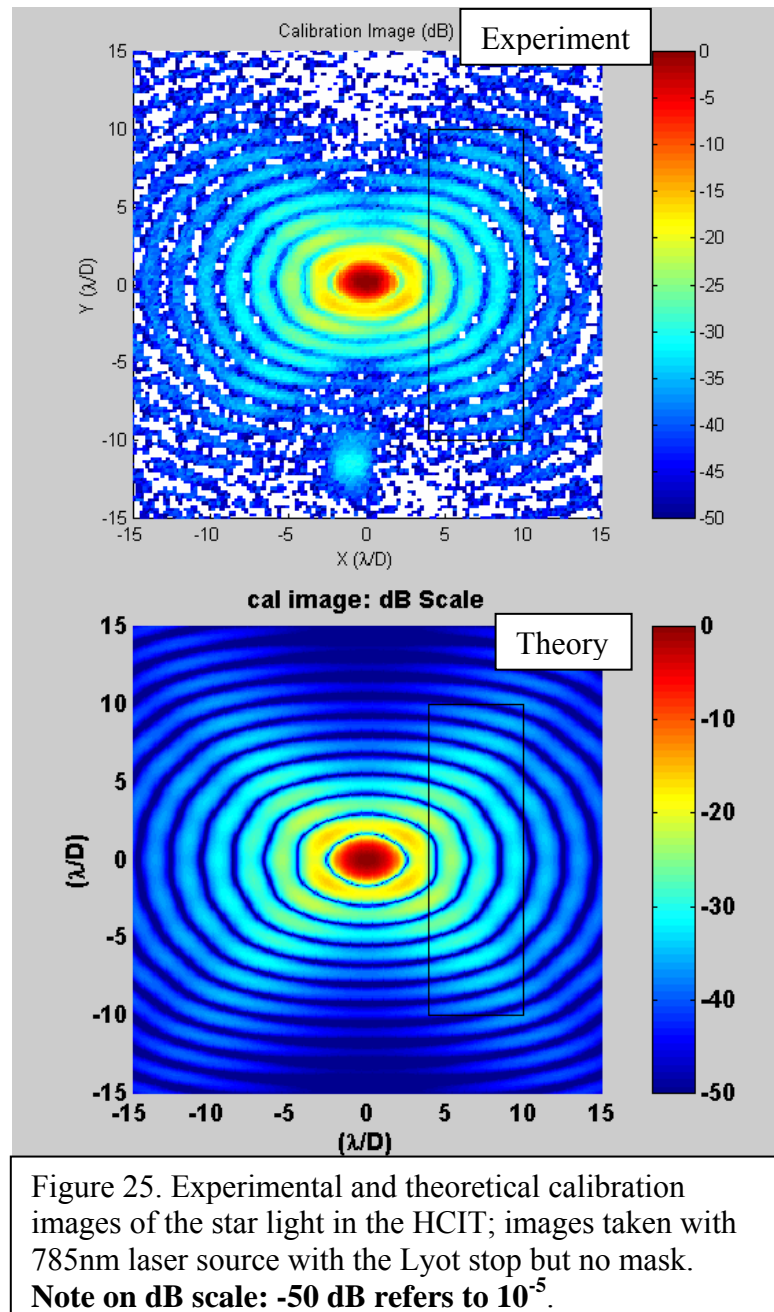
Binary Mask

The binary 1-sinc² mask was tested in the HCIT under similar conditions as with the HEBS mask. With 785nm laser light a contrast of 4×10^{-9} was obtained in the target box for a chosen polarization that was nulled with the DM while other polarization was left floating. Note that the incident light was not polarized; the light was split into orthogonal polarizations only before the final image.

Figure 25 shows the Airy patterns obtained with the Lyot stop in place but with the mask removed. The Lyot stop employed for this experiment is shown in figure 22. The top figure is the experimentally obtained calibration image in the HCIT while the bottom figure is the corresponding theoretical prediction with a perfect field assumed at the pupil. The two figures do not match perfectly, but can be considered very close because of potentially small differences between experimental conditions and simulation assumptions.

The experiment in the HCIT collected two images corresponding to the two orthogonal polarization states after the calcite crystal. Figure 26 shows the arrangement with which theoretical simulations were done with Fresnel diffraction calculations.

The following discussions and results relate to binary 1-sinc² mask with $w=157.7\mu\text{m}$ (figure 4, mask#1; figure 19, pattern 3 in layout)



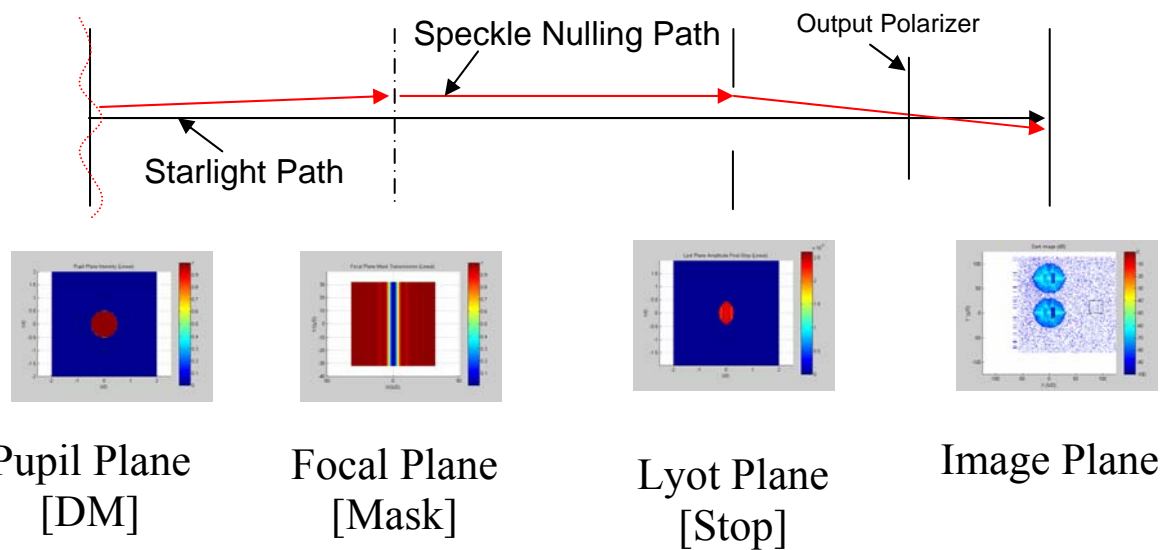


Figure 26. Conceptual layout of the coronagraph resembling the HCIT for theoretical simulation of contrast at the final image for the two orthogonal polarization states

Assumptions for the theoretical simulation:

- (1) Input polarization is wandering in time.
- (2) Images for each of the output polarizations are created by the polarizer.
- (3) One of these two images is chosen for speckle nulling.
- (4) The other image is simply recorded.
- (5) The goal is to predict the contrast in this un-nulled polarization, assuming the other polarization is nulled to its theoretical minimum.

Referring to the figure 27, where θ is the angle between the polarizer axis and the mask x axis, one can choose to null one of the polarizations perfectly through DM settings, allowing the other polarization to float. For an angle θ between the axes, the residual in the polarization being nulled is then given by

$$I_{MAIN} = |E_{yy} - E_{xx}|^2 \cos^2(\theta) \sin^2(\theta)$$

Residual in the polarization not being nulled

$$I_{CROSS} = |E_{yy} - E_{xx}|^2 [\cos^2(2\theta) + \cos^2(\theta) \sin^2(\theta)]$$

Comments:

- (1) E_{yy} and E_{xx} are computed analytically, using transmission coefficients for the mask based on a full-wave, polarization-dependent calculation.
- (2) Cross polarization from the mask is assumed to be zero, $E_{xy}=E_{yx}$.
- (3) Only for $\theta=n*\pi/2$, $n=0,1,2,..$ can the main polarization be totally nulled.
- (4) For $\theta=\pi/2$ {45 degrees} both polarizations will reach the same value.

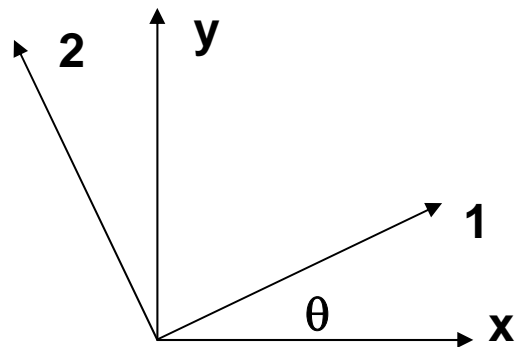


Figure 27. Polarizer x axis relative to mask x axis

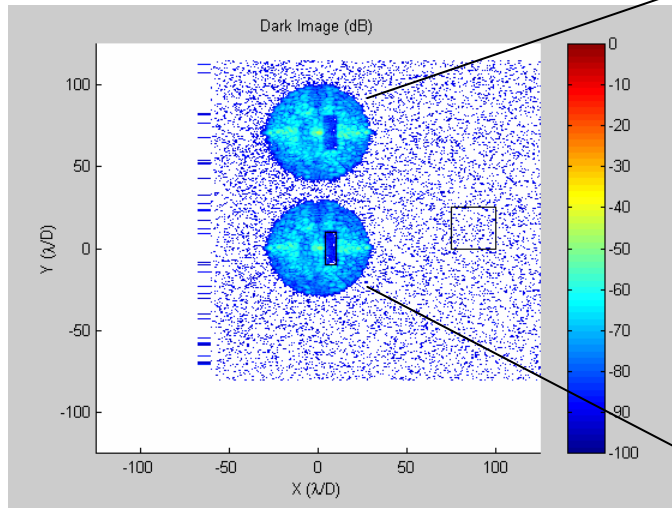


Figure 28a. Final images (Experimental) showing the two polarizations and the corresponding contrast plots from experimental data

The experimentally measured average contrast in the polarization being nulled is 4.3×10^{-9} , whereas the average contrast in the orthogonal field not nulled by DM is 1.9×10^{-8} .

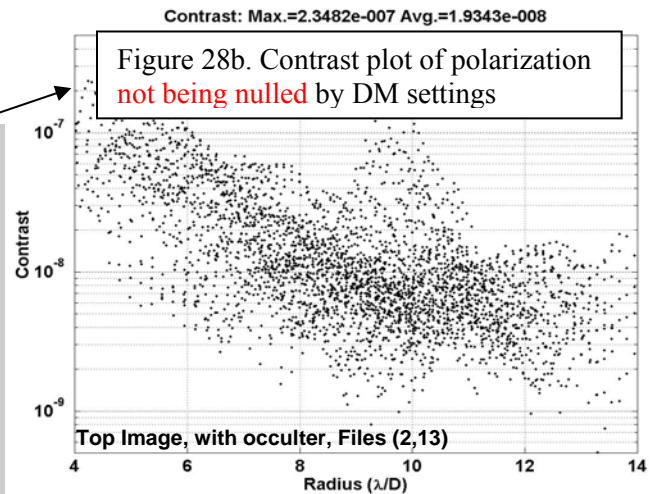


Figure 28b. Contrast plot of polarization not being nulled by DM settings

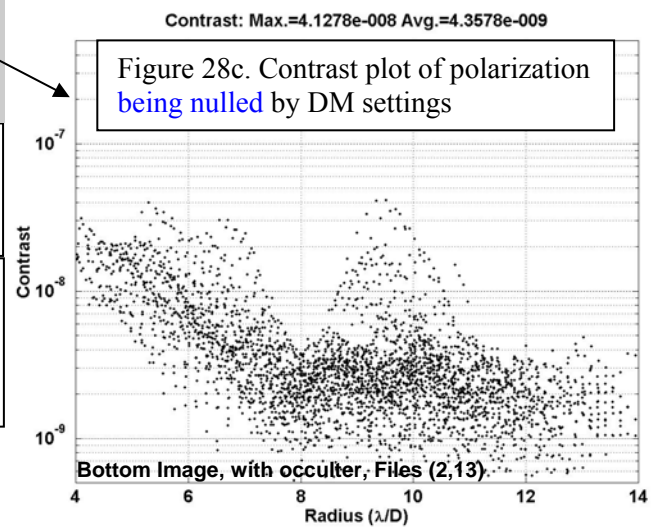


Figure 28c. Contrast plot of polarization being nulled by DM settings

Figure 28 a, b and c above show the images obtained on the HCIT for the two polarization states and the corresponding contrast plots as a function of radius in λ/D units.

The roughly 4x difference between the two polarizations is attributable to the fact that the ripples on the DM that effectively null the light inside the dark hole for one polarization would have a negative impact on the contrast achievable in the orthogonal polarization. In the case of two separate arms for the two polarizations with their own DMs, the contrast would be effectively improved to the best achievable.

Figure 29 shows the contrast plots of experimental and theoretical results for the polarization that is not nulled by the DM settings.

The better than theory results of measurements can be explained with a number of reasons.

- (1) Theoretical simulation assumes one of the fields is perfectly nulled, but in practice the nulling is effective only partially and hence the negative effect on the orthogonal field will be less than with the perfect nulling condition thereby exhibiting a better contrast than predicted.
- (2) The polarizer may not be perfect as assumed in theory.
- (3) Focus offsets in the system may also contribute to lowering the Strehl ratio (i.e., $I(0,0)$ in the contrast formula and hence the increased contrast in the calculation).

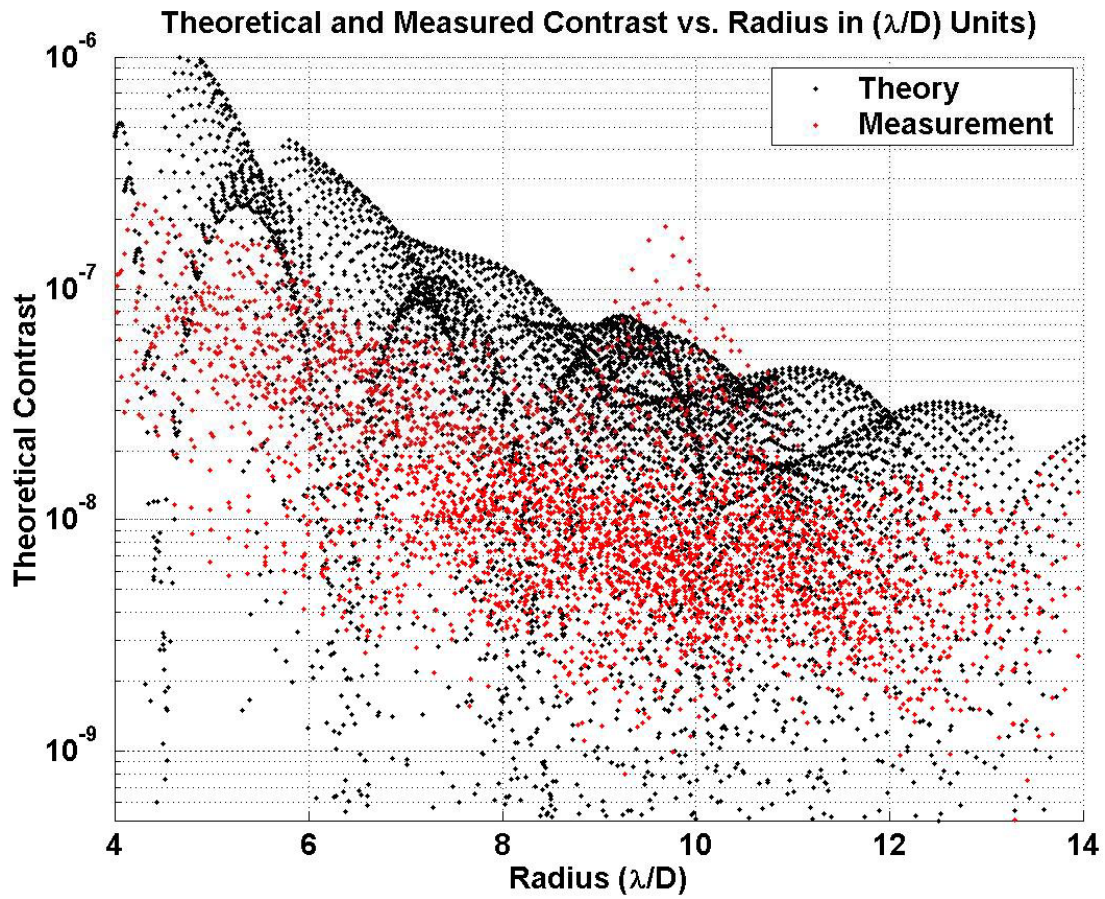
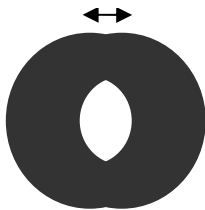


Figure 29. Computed Average Contrast Inside the Dark Hole = $5.9\text{e-}8$ {Measured $1.9\text{e-}8$ }. Note that these are for the polarization that is left floating without DM nulling. The nulled polarization would be theoretically perfectly nulled in the box, while the experiment measured the average contrast as $4.3\text{e-}9$.

Optimum Lyot stop size:

Theoretical model calculations performed with various Lyot stop dimensions are shown in figure 30. No DM is employed for these simulations. While an ideal occulter would show a sharp transition from low contrast to high contrast (red curves in figure 30), real masks with electromagnetic effects such as waveguiding, transmission losses, phase retardation and polarization effects, show an optimum Lyot size (blue curves).

Center-to-Center {1mm-13mm}



27mm diameter circles

Ideal mask's performance reaches a numerical limit somewhere between 5 and 7 mm. The physical mask has best performance near 5 mm. The airy disk of star light gets spread out into the nulled contrast box region when a narrower stop is employed and hence the contrast suffers. Performance (contrast) for the physical mask has decreased by a factor of 2.5 by using a 11mm separation vs. 5 mm. We have actually used

12mm separation for the results shown in figure 28, suggesting that there is room for Lyot stop optimization to obtain better results. It is also conceivable that the Lyot stops for the HEBS mask and binary mask have to be differently optimized due to the nature of diffraction characteristics of the two different types and they behave differently for the two orthogonal polarization fields.

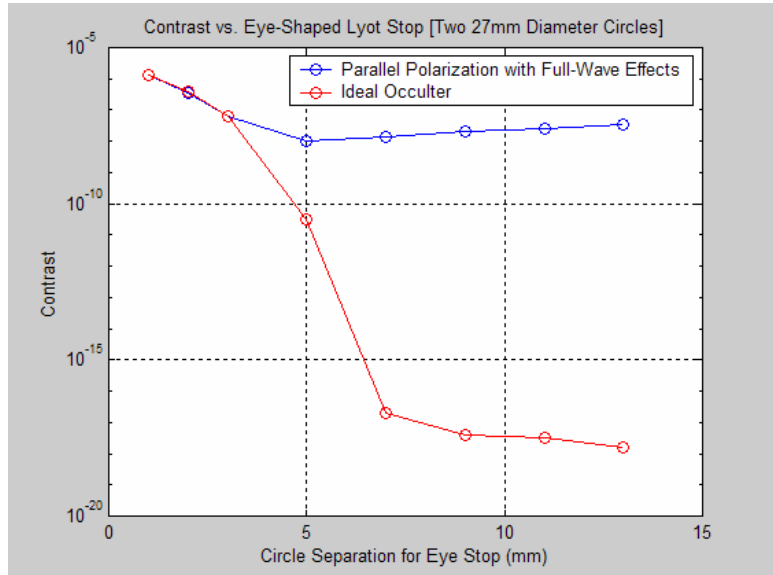
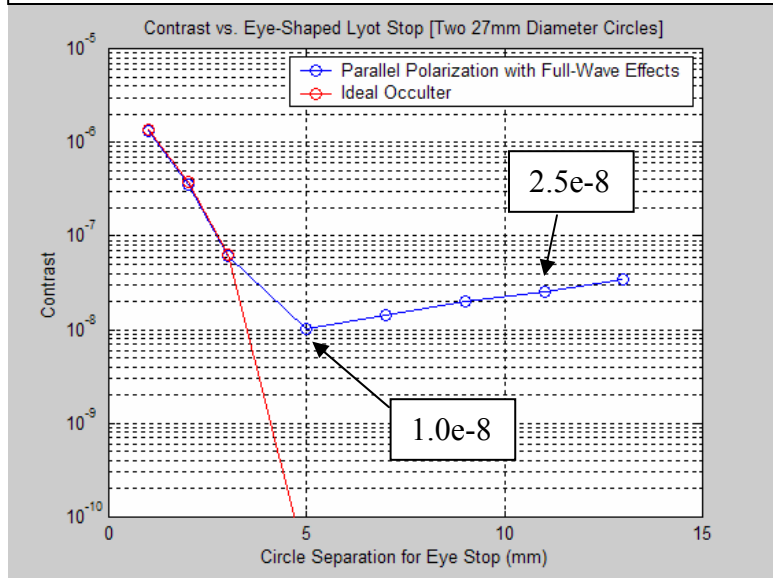


Figure 30. Contrast vs. Lyot stop dimension (separation of the two circles that make up the stop). Bottom figure: Enlarged view of top figure showing optimum separation around 5mm.



Optimum focus

Simulations suggest that the optimum focus locations for the two polarizations with the binary mask are different as shown in figure 31. Not only the best focus location is different, but the contrast achievable is also different for the two polarizations. The slightly pessimistic results of simulated predictions in figure 29 could be partly explained due to this optimum focus location. Experimental search for best focus was done for the best contrast whereas the simulations were done with zero focus offset. Note that the predictions in figure 31 are done without a DM nulling. The mask tip angle of 5 deg and the glass substrate thickness are also not included in these simulations.

As in the case of Lyot stop size, the best focus is also likely to be different between the HEBS mask and binary mask. Besides the 5 degree tip angle of the mask with respect to the beam axis and the polarization behavior of the binary mask, the substrate being different for the two masks will also partly contribute to the differences. Theoretical prediction of the difference between the two masks is a subject of on-going investigation and will guide experiments.

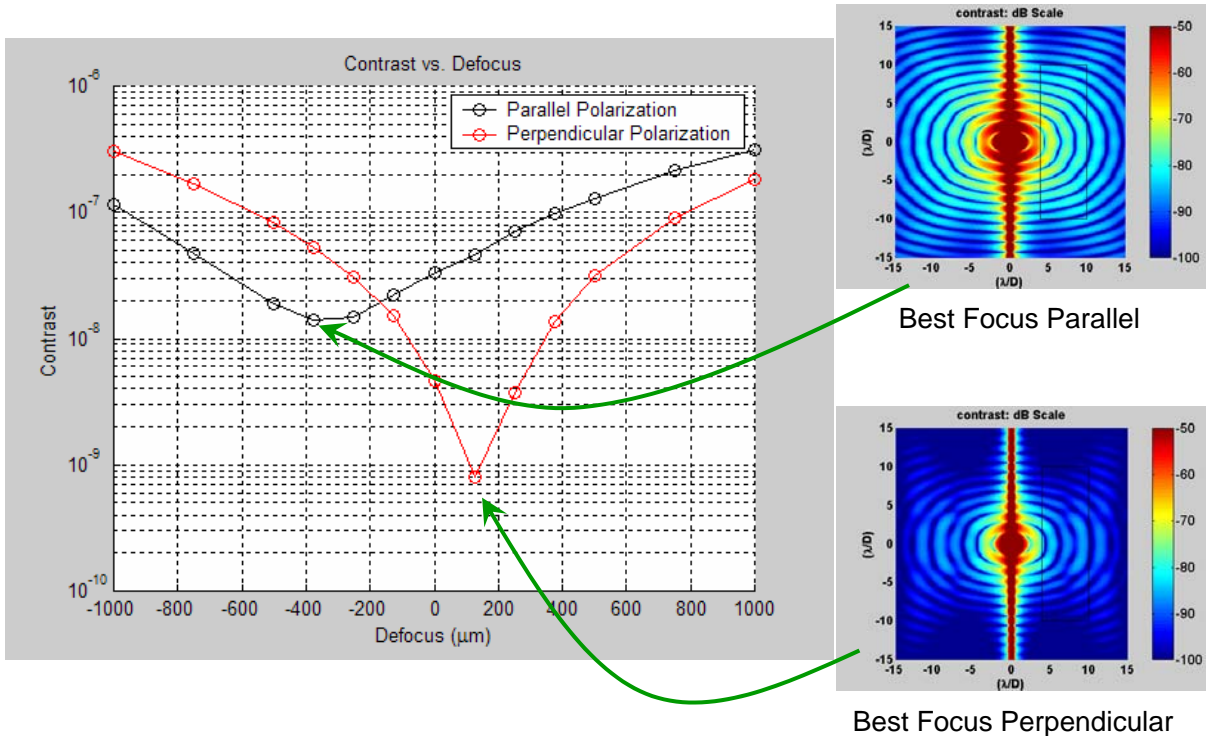


Figure 31. Contrast vs Defocus showing optimum focus locations for the two polarizations

VII. Summary

Both the HEBS and Binary masks with $1-\text{sinc}^2$ profiles have shown experimental results close to theoretical predictions. Observed differences could be explained with model assumptions and experimental conditions. Further experimental work, particularly with brighter and more stable source and controlled input polarization together with developments in the fabrication

and characterization of masks will yield better insight and improved model predictions to guide experiments.

References for further reading

Kuchner, M. J. and D.N. Spergel, “Notch Filter Masks: Practical Image Masks for Planet-Finding Coronagraphs”, *The Astrophysical Journal*, 594:617-626, 2003.

Goodman, J. W. *Introduction to Fourier Optics*, McGraw-Hill, San Francisco, 1968.

Kuchner, M.J. and W.A. Traub, “A Coronagraph with a Band-Limited Mask for Finding Terrestrial Planets”, *The Astrophysical Journal*, 570:900-908, 2003.

Trauger et al., presentation, “HCIT Coronagraph Contrast Demonstrations”, TPF/STDT meeting on Feb 24, 2005, JPL – TPF library collection 2911.

Balasubramanian, et al., HEBS Mask Material OD, Phase, Characterization, Jan. 2005, TPF library collection 1864.

Trauger et al., Coronagraph contrast demonstrations with the High Contrast Imaging Testbed, *Proc. SPIE 5487*, (2004), pp. 1330-1336; also in TPF library collection 1864.

Wilson et al., Eclipse apodization: realization of occulting spots and Lyot masks, *Proc. SPIE 4860*, (2003), pp. 361-370, also in TPF library collection 1864.

Canyon Materials, Inc. San Diego CA, <http://canyonmaterials.com>

Hoppe, D., Binary Mask Performance Predictions, July 23, 2004, TPF library collection 1864.

Hoppe, D., Full-Wave Electromagnetic Effects in Image and Pupil-Plane Masks, July 13, 2004, TPF library collection 1864.

Hoppe, D., May 5, 2005; Binary_Sinc2_Masks_DJH.doc, TPF library collection 1864.